

Determining membrane permeability of giant phospholipid vesicles from a series of videomicroscopy images

Primož Peterlin¹, Gašper Jaklič^{2,3}, and Tomaž Pisanski^{2,3}

¹University of Ljubljana, Faculty of Medicine, Institute of Biophysics, Lipičeva 2, Ljubljana, Slovenia, ²University of Ljubljana, Faculty of Mathematics and Physics, Jadranska 19, Ljubljana, Slovenia, ³University of Primorska, Primorska Institute for Natural Science and Technology, Muzejski trg 2, Koper, Slovenia

E-mail: primoz.peterlin@mf.uni-lj.si

Abstract. A technique for determining the permeability of a phospholipid membrane on a single giant unilamellar vesicle (GUV) is described, which complements the existing methods utilizing either a planar black lipid membrane or sub-micrometre-sized liposomes. A single GUV is transferred using a micropipette from a solution of a nonpermeable solute into an iso-osmolar solution of a solute with a higher membrane permeability. Osmotical swelling of the vesicle is monitored with a CCD camera mounted on a phase contrast microscope, and a sequence of images is obtained. On each image, the points on the vesicle contour are determined using Sobel filtering with adaptive binarization threshold, and from these, the vesicle radius is calculated with a great accuracy. From the time-dependence of the vesicle radius, the membrane permeability is obtained. Using a test set of data, the method provided a consistent estimate of the POPC membrane permeability for glycerol, $P = 1.7 \times 10^{-8}$ m/s, with individual samples ranging from 1.61×10^{-8} m/s to 1.98×10^{-8} m/s. This value is $\approx 40\%$ lower than the one obtained on similar systems. Possible causes for this discrepancy are discussed.

Keywords: membrane permeability, giant unilamellar vesicle, phase-contrast microscopy, image analysis

Submitted to: *Meas. Sci. Technol.*

1. Introduction

All living cells are enclosed by a lipid bilayer, which serves as a barrier for macromolecules and ions. Small uncharged molecules can, however, permeate across the membrane without requiring assistance of transmembrane proteins. Permeability of a lipid bilayer has traditionally been measured either electrically on a planar black lipid membrane [1], or optically on sub-micrometre-sized liposomes (*e.g.*, large unilamellar vesicles, LUVs), through osmotic swelling or shrinking of vesicles and a subsequent change in the light scattering [2, 3]. While these techniques have proven to be successful, they have two drawbacks. Firstly, they offer only indirect insight into the mechanism involved, and secondly, an open question remains whether the results obtained on the membranes of sub-micrometre-sized LUVs can be applied onto the

membranes of micrometre-sized giant unilamellar vesicles (GUVs), *i.e.*, whether the membrane permeability is influenced by its curvature.

In this paper, we propose a complementary technique for measuring the permeability of a lipid bilayer on GUVs using an analysis of a sequence of videomicroscopy images. Processing and analysis of digital video images acquired by an optical microscope has become an indispensable tool in biophysics, in particular for the analysis of the shape of contours of phospholipid vesicles, either free [4, 5] or aspirated in a micropipette [6].

2. Description

2.1. Experimental setup for image acquisition

In the experiment, a single spherical GUV made from 1-palmitoyl-2-oleoyl-*sn*-glycero-3-phosphocholine (POPC) was selected, fully aspirated into a glass micropipette with a diameter exceeding the diameter of the vesicle, and transferred from a solution of a solute with a very low membrane permeability (*e.g.*, glucose or sucrose) into an iso-osmolar solution of a solute with a higher membrane permeability (*e.g.*, glycerol), where the content of the micropipette was released, and the micropipette was removed. Vesicle behaviour is recorded with a CCD camera mounted on the microscope. Upon the transfer, the vesicle swells osmotically until it bursts, whereupon another cycle of swelling is commenced. The rate of swelling depends on membrane permeability and the difference of the concentration of the permeable solution outside and inside the vesicle. Since the whole sequence of the vesicle response is recorded, and the vesicle radius can be determined from micrograph images with a great precision, an estimate for the concentration difference can be obtained from the vesicle geometry, thus making an estimate of the membrane permeability possible. Vesicle transfer from a solution of a non-permeable into a solution of a permeable solute rather than vice versa, thus resulting in osmotic swelling rather than osmotic shrinking, has been chosen since it completely determines the geometry of a vesicle, *i.e.*, the vesicle is spherical throughout the experiment, thus making a high-precision measurement of its radius possible. The micromanipulation experiment is explained in detail in [7].

The experimental setup consisted of a phase contrast inverted optical microscope (Nikon Diaphot 200, objective 20/0.40 Ph2 DL; Tokyo, Japan) with the micromanipulating equipment (Narishige MMN-1/MMO-202; Tokyo, Japan) and a cooled CCD camera (Hamamatsu ORCA-ER; C4742-95-12ERG; Hamamatsu, Japan), connected via IEEE-1394 to a PC running Hamamatsu Wasabi software. The camera provides 1344×1024 12-bit grayscale images. In the streaming mode, the camera throughput is 8.9 images/s. Even though custom solutions have been shown to provide a higher throughput in similar cases [8], the software supplied by the manufacturer was proved to be adequate for the camera.

2.2. The model for vesicle inflation and burst

The basic ideas of the model explaining the swelling-burst cycle will be presented first. After the transfer, a spherical vesicle filled with an impermeable solute is immersed in a solution of a permeable solute. Since the concentration of the permeable solute outside the vesicle (c_{p0}) exceeds its concentration inside the vesicle (c_p), it tends to diffuse into the vesicle. During this phase, the amount of the impermeable solute inside the vesicle

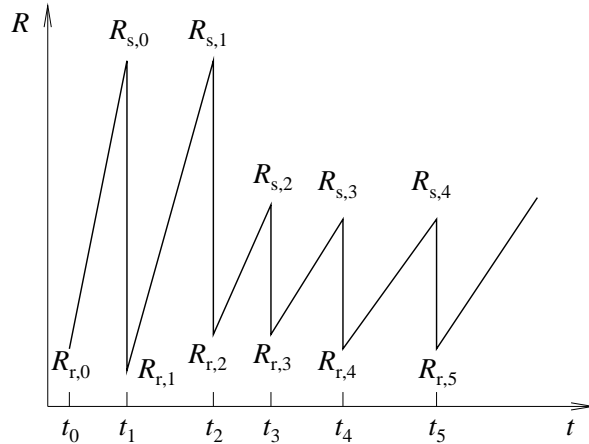


Figure 1. A schematic indication of the vesicle radius R as a function of time t upon transfer from a solution of an impermeable solute into an iso-osmolar solution of a permeable solute.

(N_i) remains constant, while the amount of the permeable solute (N_p) increases. Its influx is accompanied by an influx of water required to maintain the osmotic balance. Based on the known data [1], it is assumed in this model that the permeability of the membrane for water exceeds all other permeabilities by several orders of magnitude, and consequently the osmotic balance is achieved almost instantly. Consequently, in order to maintain the osmotic balance, the vesicle volume increases as well. In an instantaneous event of a vesicle burst, a fraction of the solution is ejected from the vesicle interior. During the burst, the concentration of both solutes (c_p , c_i) inside the vesicle stays constant, while their amount decreases, the decrease being proportional to the decrease of the vesicle volume. The cycle then repeats itself with new values of the concentrations c_p and c_i . The theory of the osmotic inflation–burst cycle is described in more detail in [9, 10, 7].

The flux of the permeable solute into the vesicle (j) is proportional to the difference of the concentration of permeable solute outside (c_{p0}) and inside (c_p) the vesicle,

$$j = P(c_{p0} - c_p), \quad (1)$$

where P is the permeability of the membrane for the permeable solute. The number of its molecules inside the vesicle (N_p) increases with time at a rate:

$$\frac{dN_p}{dt} = PA \left(c_{p0} - \frac{N_p}{V} \right). \quad (2)$$

Both the vesicle volume V and the membrane area A vary with time, which means that in general, (2) can only be solved numerically.

For realistic parameter values, however, numerical integration is not needed. It is known [11] that the lipid membrane can only expand by approximately 4% before its tensile strength is reached (“stretched” radius R_s), at which point the vesicle bursts and ejects its excess volume, and its radius R returns to its “relaxed” value R_r (figure 1).

Such small changes of R can be linearized, leading to a linear dependence of V in the time between bursts. A rearrangement of Eq. 11 in [7] yields a relation between

the rate of the volume increase in the n -th cycle, $\Delta V_n/\Delta t_n$, and the concentration of the impermeable solute in the vesicle during this cycle, $N_i^{(n)}$:

$$\frac{\Delta V_n}{\Delta t_n} := \frac{V_{s,n} - V_{r,n}}{t_{n+1} - t_n} = \frac{3P}{R_{r,0}} \frac{N_i^{(n)}}{c_{p0}}. \quad (3)$$

We have denoted $V_{r,n} = 4\pi R_{r,n}^3/3$ and $V_{s,n} = 4\pi R_{s,n}^3/3$.

While t_n , $R_{r,n}$ and $R_{s,n}$ can be determined directly, the value of $N_i^{(n)}$ at the n -th burst can be calculated. Since the amount of the impermeable solute inside the vesicle remains constant during the time between successive bursts, one can write:

$$\begin{aligned} N_i^{(0)} &= c_i^{(0)} V_{r,0} = c_i^{(1)} V_{s,0}, \\ N_i^{(1)} &= c_i^{(1)} V_{r,1} = c_i^{(2)} V_{s,1}, \\ &\dots \end{aligned} \quad (4)$$

From here, a general expression for $c_i^{(n)}$ can be obtained:

$$c_i^{(n)} = c_i^{(0)} \prod_{j=0}^{n-1} \frac{V_{r,j}}{V_{s,j}}. \quad (5)$$

The initial amount of the impermeable solute inside the vesicle is known, $N_i^{(0)} = V_{r,0} c_i^{(0)}$. We also know that the solutions inside and outside the vesicle are iso-osmolar ($c_i^{(0)} = c_{p0}$). Taking into account that the relaxed radii of the vesicle are approximately equal ($V_{r,n} \approx V_{r,0}$), and substituting this into (3), one obtains:

$$\frac{\Delta V_n}{\Delta t_n} = P 4\pi R_{r,0}^2 \prod_{j=0}^{n-1} \frac{V_{r,j}}{V_{s,j}}. \quad (6)$$

Thus, plotting $\Delta V_n/\Delta t_n$ against $4\pi R_{r,0}^2 \prod_{j=0}^{n-1} V_{r,j}/V_{s,j}$, one should obtain a straight line with the slope equal to P .

2.3. Determining vesicle radius from a videomicrograph

Phase contrast micrographs exhibit a distinct ‘‘halo’’, if the index of refraction of the medium inside does not match the refractive index of the medium outside [12].

A Sobel edge detection operator [13] was used to determine the radius of the vesicle. The choice of threshold of the binarization applied to the image after the convolution affects the result in an important way. Since the contrast of the halo decreases throughout the time of recording, the binarization threshold needs to be adjusted dynamically in order to yield the desired result (figure 2). The binarization threshold was selected on the basis of the number of points it yields, in a way that the number of points making up the contour was between $2\pi R/3$ and $2\pi R$, where R is the running average of previously determined values, expressed in pixels. In this interval, the calculated radius is virtually independent of the number of points taken into calculation (figure 3).

A circle with a centre (x_c, y_c) and a radius R is fitted to a set of n points (x_i, y_i) obtained in the previous step. A computationally efficient algorithm for fitting a general conic to a set of data points [14] was adapted specifically for fitting ellipses [15]. It turns out that the system obtained in [15] is unstable, *e.g.*, the approach does not work for the data, sampled from a circle. A more stable and efficient modification has been proposed by Halíř and Flusser [16].

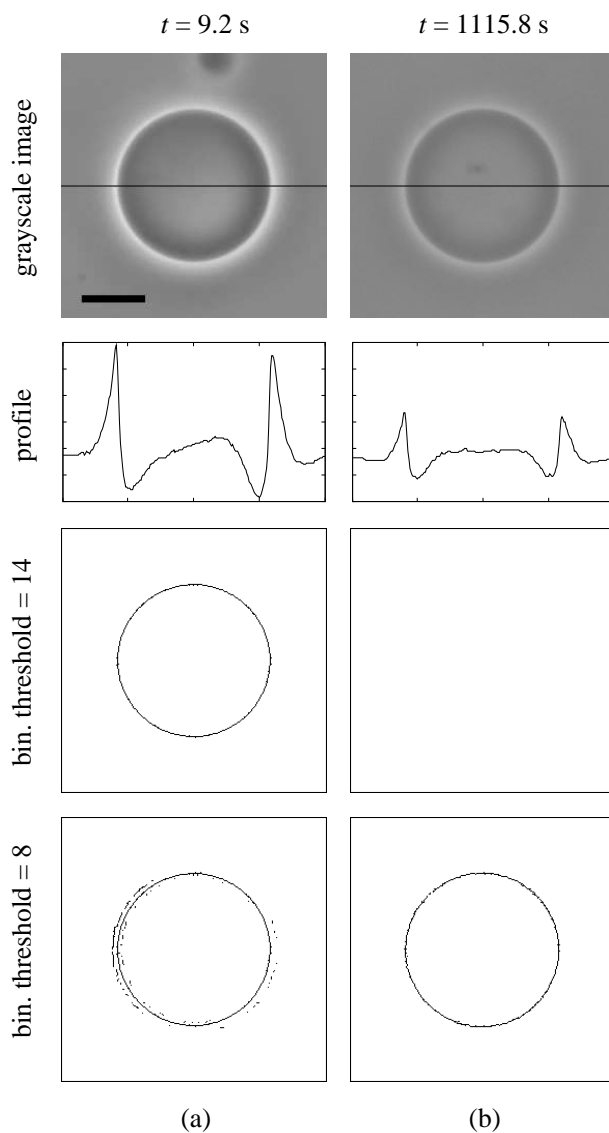


Figure 2. Adaptive Sobel threshold. As the composition of the solution in the vesicle interior approaches the composition of the vesicle exterior, the contrast fades from videomicrograph frames taken at the beginning of the experiment (a, top row) to frames taken towards the end of the experiment (b, top row); the second row shows the intensity profile of the vesicle cross-section shown in the same scale. It is thus necessary to dynamically adjust the binarization threshold of the Sobel edge operator. High values of threshold, which produce an acceptable image at the beginning of the experiment (a, third row), fail to discriminate the edge towards the end of the experiment (b, third row). On the other hand, low values of threshold, which are appropriate for the image frames towards the end of the experiment (b, bottom row) produce stray points at the beginning of the experiment. The algorithm for the dynamical adjustment of the binarization threshold selects an image corresponding to the one in the third row for (a), and an image corresponding to the one in the fourth row for (b). The bar in the top left frame represents $20 \mu\text{m}$.

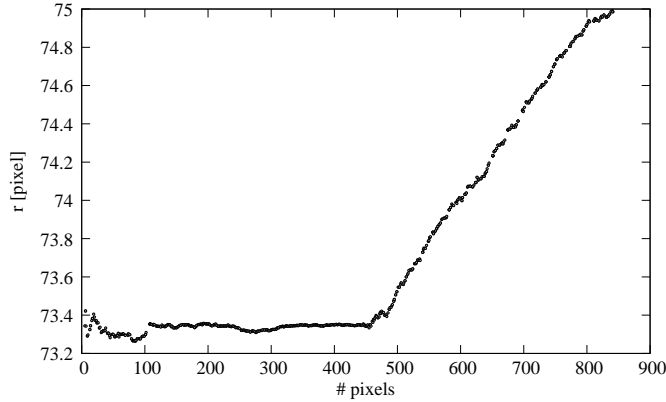


Figure 3. For a given image, the calculated radius of a vesicle depends on the number of points taken into consideration. When the binarization threshold is very high, very few points are selected and the calculated radius is significantly affected by any new point taken into consideration. In an intermediate region, the calculated radius does not depend on the number of points. Above a certain threshold value, spurious points taken into consideration affect the calculated radius. The data plotted are for the image plotted in figure 2a; the interval $[2\pi R/3, 2\pi R]$ approximately translates to $[150, 460]$, corresponding to the interval $[9.90, 22.60]$ for the binarization threshold.

Further simplification can be employed for fitting circles, which reduces the problem to solving a linear 3×3 system rather than solving a generalized eigenvalue problem, as required in [15]. If the matrix \mathbf{A} and the vector \mathbf{b} are constructed as follows:

$$\mathbf{A} = \begin{bmatrix} \sum_i x_i^2 & \sum_i x_i y_i & \sum_i x_i \\ \sum_i x_i y_i & \sum_i y_i^2 & \sum_i y_i \\ \sum_i x_i & \sum_i y_i & n \end{bmatrix}, \quad (7)$$

$$\mathbf{b} = \begin{bmatrix} \sum_i x_i (x_i^2 + y_i^2) \\ \sum_i y_i (x_i^2 + y_i^2) \\ \sum_i (x_i^2 + y_i^2) \end{bmatrix}, \quad (8)$$

then the required parameters are stored in a vector $\mathbf{v} = (v_1, v_2, v_3)$, obtained as the solution of a set of linear equations,

$$\mathbf{A} \cdot \mathbf{v} = \mathbf{b}. \quad (9)$$

In particular,

$$x_c = \frac{1}{2}v_1, \quad (10)$$

$$y_c = \frac{1}{2}v_2, \quad (11)$$

$$R = \sqrt{x_c^2 + y_c^2 + v_3}. \quad (12)$$

The matrix \mathbf{A} in (7) is positive definite, provided that at least 3 data points are non-collinear. This can be easily seen from the factorization $\mathbf{A} = \mathbf{C}^T \mathbf{C}$, where $\mathbf{C} := [\mathbf{x} \ \mathbf{y} \ \mathbf{1}]$ with vectors of data points \mathbf{x} , \mathbf{y} , and a vector of ones $\mathbf{1}$. Note that the set of linear equations (9), even though derived by a different procedure, is equivalent to the one obtained by Kása [17] by a modified least square criterion, *i.e.*, by minimizing

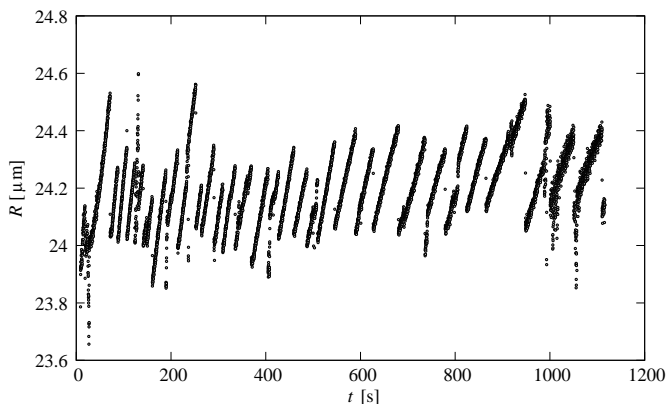


Figure 4. The determined vesicle radius R as a function of time t upon a transfer from a 0.2 mol/L sucrose/glucose solution into an iso-osmolar glycerol solution.

the sum $\sum_i [(x_i - x_c)^2 + (y_i - y_c)^2 - R^2]^2$. We would like to remark that a great deal of research has been done on the approximation of circular arcs and whole circles (see, *e.g.*, [18] and the references therein). Since in our case the vesicle contour is known to have circular shape, special polynomial or spline approximations are not needed.

A script was written in GNU Octave (<http://www.octave.org/>, [19]), a Matlab-compatible software package, to determine the radius of the vesicle from a videomicrograph image. Figure 4 shows a series of calculated radii from an 18-minute recording of a vesicle. As verified by a visual inspection, occasional apparent transient increases or decreases of the radius are due to image defocussing (as the cover slide, along which vesicles move, is not perfectly aligned with the focal plane, the experimentalist needs to occasionally adjust the focussing knob on the microscope in order to assure that the vesicle is still in focus). Such transient changes in the apparent calculated vesicle radius occur on an a time-scale of seconds and it is thus easy to discriminate them against real changes of vesicle radius.

Another GNU Octave script was used to read the output of the first script, *i.e.*, the vesicle radius as a function of time, and determine the points at which vesicle bursts occurred. The algorithm employed was a simple one: the script looked for negative jumps in vesicle radius, the magnitude of which exceeded some pre-determined value and which did not follow the previous jump too soon. Both parameters—the minimum amplitude and the minimum time interval between the jumps—were hand-tailored to fit the experimental data. Using this algorithm, 90–95% of the jumps were detected; the missing ones were added by hand upon comparing the results to the data.

3. Results and Discussion

3.1. Test set of data

The algorithm was tested on a set of data used in [7] (figure 5). Membrane permeability has been calculated for four recorded series of bursts (vesicles 2–5 in table 1, [7]), yielding an average value $P = 1.7 \times 10^{-8}$ m/s at a room temperature ($26 \pm 2^\circ\text{C}$), with the estimates on individual vesicles ranging from 1.61×10^{-8} m/s to 1.98×10^{-8} m/s. This value is lower than the value $(2.09 \pm 0.82) \times 10^{-8}$ m/s obtained in [7] by another

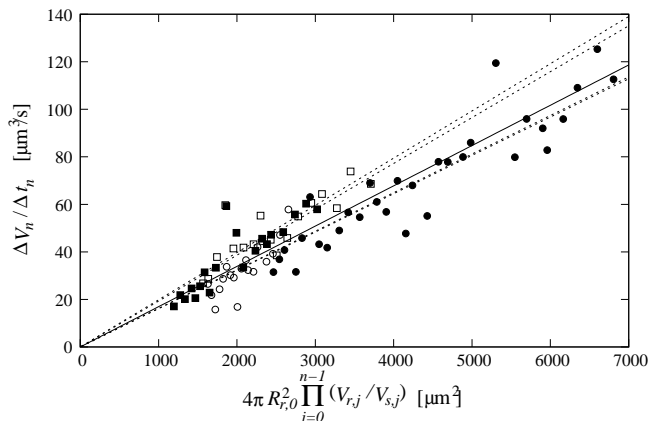


Figure 5. The rate of the volume increase $\Delta V_n/\Delta t_n$ plotted against $4\pi R_{r,0}^2 \prod_{j=0}^{n-1} V_{r,j}/V_{s,j}$, shown for four different vesicles transferred from 0.2 mol/L glucose/sucrose into 0.2 mol/L glycerol (denoted \circ (19 points), \bullet (31 points), \square (17 points), and \blacksquare , 20 points). Least-squares fitting of a straight line through the origin yields values of P $(1.61 \pm 0.07) \times 10^{-8}$ m/s, $(1.62 \pm 0.04) \times 10^{-8}$ m/s, $(1.98 \pm 0.07) \times 10^{-8}$ m/s, and $(1.93 \pm 0.08) \times 10^{-8}$ m/s, respectively (plotted with a dotted line; the lower two lines are barely distinguishable). Here, the slope of a straight line through n points (x_i, y_i) is calculated as $m = \sum_i x_i y_i / \sum_i x_i^2$, and its standard error as $\sum_i (y_i - m x_i)^2 / ((n-1) \sum_i x_i^2)$. A solid line fitted through all four sets of points corresponds to $P = (1.69 \pm 0.03) \times 10^{-8}$ m/s.

method on the same data set, as well as from other published data, *e.g.*, the value for DOPC, 2.75×10^{-8} m/s at 30°C [3], and two values for egg-PC, $(4.3 \pm 0.1) \times 10^{-8}$ m/s [20] and 5.4×10^{-8} m/s at 25°C [21].

One has to note, however, that the only result against which we can directly compare the obtained result is the one obtained by a different analysis on the same data set [7]. Both results agree within the margins of standard error in [7]. All other results were obtained on systems which were different, even though they share some similarities. Paula *et al.* [3] did not include POPC in their measurement. The most similar system of those included is DOPC, which has two unsaturated acyl chains (POPC has one unsaturated and one saturated chain). It is known that increasing chain saturation decreases membrane fluidity, and membrane fluidity has been shown to be well-correlated with the permeability of membrane for small uncharged solutes [22]. Furthermore, the experiment has been conducted at a slightly higher temperature, and it is known that membrane permeability scales with temperature approximately as Arrhenius factor, $\propto \exp(-E_a/kT)$ [23].

The other two measurements [20, 21] were conducted on natural egg phosphatidylcholine. According to the specifications provided by the producer (Avanti Polar Lipids, Inc.), this is a mixture of various lipids, both saturated and unsaturated, ranging in length of the acyl chain from 16 to 20 carbon atoms. It is to be expected that a heterogenous membrane has a higher permeability, and indeed, the permeabilities of egg-PC membrane listed in [20, 21] are consistently higher than those for DOPC membrane listed in [3].

As one can see, the presented method offers a possibility to determine membrane permeability with a relative accuracy comparable to or greater than other published results. Based on the above argumentation, one could expect that the value obtained

for permeability of POPC membrane should be slightly lower than the published values for other similar systems, and indeed it is. We have not shown, however, that the extent of the observed discrepancy can be explained solely by the fact that we were working with a different system. We can think of several possible additional factors which could also affect the estimated permeability.

Firstly, this discrepancy may indicate that the membrane permeability depends on the membrane curvature and thus one may indeed expect different values for the membrane of GUVs, which are essentially planar, than for the membranes of LUVs and other smaller aggregates. A comparison by Brunner *et al.* [24] however shows that planar membranes (black lipid membranes, BLM) exhibited higher permeabilities for ions and sugars than the membranes of sonicated small unilamellar vesicles (SUVs); it is to be noted, though, that the authors report problems with leakage and attribute a comparatively high value for BLM permeability to this artefact.

Secondly, it may be due to the fact that the model presented in section 2.2 does not take into account the membrane elasticity. It has already been pointed out [25] that failing to account for membrane elasticity in the interpretation of the membrane permeability measurements in a similar experiment leads to an underestimate of membrane permeability. Our earlier estimates [7] however show that this correction amounts to only 2–3% and thus cannot explain the observed difference.

Thirdly, the apparent value of permeability, as obtained in the experiment, is coupled with the diffusion of the permeable solute through the stagnant layer [26] and is therefore lower than the true permeability of the membrane alone. A quick estimate however shows that the effect of the stagnant layer only affects the calculated permeability to a few percent.

Finally, one has to bear in mind that the phase contrast technique does not yield the true position of the vesicle membrane. Instead, we have to rely on the “halo”, which is an artefact of the technique, and define the position of the membrane as the point of the maximal gradient of the image intensity. For a straight-edge object, it has been calculated [27] that the maximal steepness of the profile slope indeed coincides with the position of the edge. A rigorous theoretical treatment would require repeating this calculation for each vesicle, taking into account the real parameters of the optical system used, which would considerably complicate the analysis without a promise of a significant improvement. As a consequence, even the most precise analyses of vesicle contours to date [28, 29] dismiss this discrepancy as negligible and rely to the result of Wilson and Sheppard [27]. All in all, we can conclude that the method presented in this paper needs to be applied to a wider variety of systems before this feature can be fully explained, and then possibly applied to other interesting phenomena, such as the critical phenomena predicted [30].

3.2. Comparison with other halo-based techniques

Although it is based on previous works [10, 7], the presented technique uses a different method for determining the composition of the vesicle interior, *i.e.*, the amount of the impermeable solute $N_1^{(n)}$. The previously published methods relied on the height of the “halo” of the phase-contrast image for determining the composition of the vesicle interior and tacitly assumed that all the jumps of the vesicle radius were equal. Figure 4 demonstrates that this is not necessarily the case. Furthermore, since no *ab initio* calculation of the “halo” profile has been done, the authors in [10] and [7] had to resort to the calibration of the halo. As the halo profile depends not only on

the refractive indexes of the solutions in the vesicle interior and the vesicle exterior, but also on the size of the vesicle and, in absolute terms, on the properties of the optical system used (*e.g.*, a slight displacement of the phase ring from the optical axis affects it considerably), this analysis is cumbersome, and any laboratory trying to apply this technique needs to repeat the calibration on their system. By replacing the need for the measurements of the halo properties such as its height or width with a more precise measurements of the vesicle radius, which enables us to estimate the composition of the vesicle interior using simple geometry (6), we eliminated the need for the cumbersome calibration altogether, and thus made the technique much more portable. A further advantage is that shedding the reliance on the quantitative properties of the halo also opens the possibility for using techniques for improving uneven illumination (see, *e.g.*, [31]), if necessary. Note, however, that when using the presented technique, it is important to record the vesicle behaviour right from the time of the transfer, as missing a burst yields to underestimating the permeability.

Applying the technique from [10] to the measurement of small polar molecules, as has been done in [7], introduces a further problem, since the calibration itself involves a tricky part—the experimentalist has to determine a suitable point for the initial concentration difference, *i.e.*, a point late enough that the amount of the initial solution transferred with the micropipette along with the vesicle has diffused away enough not to affect the refracting index of the external solution significantly, and early enough that the amount of the permeable solute which has entered the vesicle can still be neglected. This procedure requires some experience and can not be automated. This does not present a problem with the experiment where membrane permeability due to peptide incorporation in the membrane is studied [10], as the permeability of membrane in the absence of peptides is very low and the experimentalist has plenty of time for the calibration. As the technique presented here does not rely on the properties of the halo profile, it provides a better alternative for measuring the permeability of membrane for small polar molecules.

4. Conclusions

We describe a technique for determining the permeability of a phospholipid membrane of micrometre-sized GUVs from a sequence of videomicrographs, which complements the existing methods of determining membrane permeability on either sub-micrometre-sized liposomes (SUV, LUV) or planar membranes. The technique relies on determining the radius of a spherical GUV with a great precision, and offers a substantial improvement over similar techniques which rely on quantifying the properties of the phase-contrast halo such as the height or width of its profile. When applied to a test set of data, the technique yielded consistent results. The obtained value is, however, $\approx 40\%$ lower than the results obtained on similar systems. Further investigations on a system comparable to the ones in the literature are needed to determine whether this discrepancy would still persist.

Acknowledgments

The authors would like to thank V. Arrigler for her skillful help with phospholipid vesicles, and M. Raič and M. Pisanski for a helpful discussion. This work has been supported by the Slovenian Research Agency through grants P1-0055 (PP) and P1-0294 (GJ, TP).

References

- [1] Anne Walter and John Gutknecht. Permeability of small nonelectrolyte molecules through lipid bilayer-membranes. *J. Membrane Biol.*, 90(3):207–217, 1986.
- [2] J. de Gier. Osmotic behaviour and permeability properties of liposomes. *Chem. Phys. Lipids*, 64:187–196, 1993.
- [3] Stefan Paula, A. G. Volkov, A. N. Van Hoek, T. H. Haines, and David W. Deamer. Permeation of protons, potassium ions, and small polar molecules through phospholipid bilayers as a function of membrane thickness. *Biophys. J.*, 70:339–348, 1996.
- [4] H. Engelhardt, H. P. Duwe, and E. Sackmann. Bilayer bending elasticity measured by Fourier-analysis of thermally excited surface undulations of flaccid vesicles. *J. Physique Lett.*, 46(8):L395–L400, 1985.
- [5] S. Seul, M. J. Sammon, and L. R. Monar. Imaging of fluctuating domain shapes – methods of image-analysis and their implementation in a personal computing environment. *Rev. Sci. Instrum.*, 62(3):784–792, 1991.
- [6] Volkmar Heinrich and Wiesława Rawicz. Automated, high resolution micropipet aspiration reveals new insight into the physical properties of fluid membranes. *Langmuir*, 21:1962–1971, 2005.
- [7] Primož Peterlin and Vesna Arrigler. Electroformation in a flow chamber with solution exchange as a means of preparation of flaccid giant vesicles. *Colloid. Surface. B*, 64:77–87, 2008.
- [8] Hisashi Fujiwara, Masayuki Mori, and Takashi Ishiwata. Continuous acquisition and storage of uncompressed image data based on a personal computer equipped with a CCD camera and an external hard disk drive. *Meas. Sci. Technol.*, 18:952–958, 2007.
- [9] M. M. Koslov and V. S. Markin. A theory of osmotic lysis of lipid vesicles. *J. Theor. Biol.*, 109:17–39, 1984.
- [10] Mojca Mally, Janja Majhenc, Saša Svetina, and Boštjan Žekš. Mechanisms of equinatoxin II-induced transport through the membrane of a giant phospholipid vesicle. *Biophys. J.*, 83(2):944–953, 2002.
- [11] M. Bloom, Evan Evans, and O. G. Mouritsen. Physical properties of the fluid lipid-bilayer component of cell-membranes—a perspective. *Q. Rev. Biophys.*, 24(3):293–397, 1991.
- [12] Maksymilian Pluta. *Advanced Light Microscopy*, volume 2. Specialized Methods, chapter 5, pages 15–20. Elsevier, Amsterdam, 1989.
- [13] Rafael C. Gonzalez and Richard E. Woods. *Digital Image Processing*, chapter 10. Prentice Hall, Upper Saddle River, NJ, USA, 2nd edition, 2002.
- [14] Fred L. Bookstein. Fitting conic sections to scattered data. *Comput. Vision Graph.*, 9(1):56–71, 1979.
- [15] Andrew Fitzgibbon, Maurizio Pilu, and Robert B. Fisher. Direct least square fitting of ellipses. *IEEE Trans. Pattern Anal.*, 21(5):476–480, 1999.
- [16] Radim Halír and Jan Flusser. Numerically stable direct least squares fitting of ellipses. In Václav Skala, editor, *Proc. 6th Int. Conf. Central Eur. Comput. Graph. Visual.*, volume I, pages 125–132, Plzeň, Czech Republic, February 9–13 1998. University of West Bohemia.
- [17] I. Kása. A circle fitting procedure and its error analysis. *IEEE Trans. Instrum. Meas.*, 25:8–14, 1976.
- [18] Gašper Jaklič, Jernej Kozak, Marjeta Kranjc, and Emil Žagar. On geometric interpolation of circle-like curves. *Comput. Aided Geom. Design*, 24(5):241–251, 2007.
- [19] John W. Eaton. *GNU Octave manual*. Network Theory Ltd., Bristol, UK, 2nd edition, 2002. Available from <http://www.octave.org/>.
- [20] C. Dordas and P. H. Brown. Permeability of boric acid across lipid bilayers and factors affecting it. *J. Membrane Biol.*, 175:95–105, 2000.
- [21] Eli Orbach and Alan Finkelstein. The nonelectrolyte permeability of planar lipid bilayer. *J. Gen. Physiol.*, 75:427–436, 1980.
- [22] Marc B. Lande, Joanne M. Donovan, and Mark L. Zeidel. The relationship between membrane fluidity and permeability to water, solutes, ammonia, and protons. *J. Gen. Physiol.*, 106(1):67–84, 1995.
- [23] F. W. Kleinhans. Membrane permeability modeling: Kedem-Katchalsky vs a two-parameter formalism. *Cryobiology*, 37:271–289, 1998.
- [24] Josef Brunner, David E. Graham, Helmut Hauser, and Giorgio Semenza. Ion and sugar permeabilities of lecithin bilayers: Comparison of curved and planar bilayers. *J. Membrane Biol.*, 57(2):133–141, 1980.
- [25] Shivkumar Chiruvolu and Joseph A. N. Zasadzinski. Membrane elasticity effects on permeability measurements in vesicles. *AIChE J*, 39(4):647–652, 1993.

- [26] Peter H. Barry and Jared M. Diamond. Effects of unstirred layers on membrane phenomena. *Physiol. Rev.*, 64(3):763–872, 1984.
- [27] Tony Wilson and Colin J. R. Sheppard. The halo effect of image processing by spatial frequency filtering. *Optik*, 59(1):19–23, 1981.
- [28] Hans-Günther Döbereiner, Evan Evans, Martin Kraus, Udo Seifert, and Michael Wortis. Mapping vesicle shapes into the phase diagram: A comparison of experiment and theory. *Phys. Rev. E*, 55(4):4458–4474, 1997.
- [29] Jacques Pécéréaux, Hans-Günther Döbereiner, Jacques Prost, Jean-François Joanny, and Patricia Bassereau. Refined contour analysis of giant unilamellar vesicles. *Eur. Phys. J. E*, 13:277–290, 2004.
- [30] Emir Haleva and Haim Diamant. Critical swelling of particle-encapsulating vesicles. *Phys. Rev. Lett.*, 101:078104, 2008.
- [31] Boštjan Likar, J. B. Antoine Maintz, Max A. Viergever, and Franjo Pernuš. Retrospective shading correction based on entropy minimization. *J. Microsc.*, 197:285–295, 2000.